

PCCP

Accepted Manuscript



This is an *Accepted Manuscript*, which has been through the Royal Society of Chemistry peer review process and has been accepted for publication.

Accepted Manuscripts are published online shortly after acceptance, before technical editing, formatting and proof reading. Using this free service, authors can make their results available to the community, in citable form, before we publish the edited article. We will replace this *Accepted Manuscript* with the edited and formatted *Advance Article* as soon as it is available.

You can find more information about *Accepted Manuscripts* in the [Information for Authors](#).

Please note that technical editing may introduce minor changes to the text and/or graphics, which may alter content. The journal's standard [Terms & Conditions](#) and the [Ethical guidelines](#) still apply. In no event shall the Royal Society of Chemistry be held responsible for any errors or omissions in this *Accepted Manuscript* or any consequences arising from the use of any information it contains.

Physical chemistry and membrane properties of two phosphatidylinositol bisphosphate isomers[†]

David R. Slochower,^{*a,b} Yu-Hsiu Wang,^a Ravi Radhakrishnan,^{a,b} and Paul A. Janmey^{a,c}

Received Xth XXXXXXXXXXXX 20XX, Accepted Xth XXXXXXXXXXXX 20XX

First published on the web Xth XXXXXXXXXXXX 200X

DOI: 10.1039/b000000x

The most highly charged phospholipids, polyphosphoinositides, are often involved in signaling pathways that originate at cell-cell and cell-matrix contacts, and different isomers of polyphosphoinositides have distinct biological functions that cannot be explained by separate highly specific protein ligand binding sites [Lemmon, *Nature Reviews Molecular and Cell Biology*, 2008, **9**, 99-111]. PtdIns(3,5)P₂ is a low abundance phosphoinositide localized to cytoplasmic-facing membrane surfaces, with relatively few known ligands, yet PtdIns(3,5)P₂ plays a key role in controlling membrane trafficking events and cellular stress responses that cannot be duplicated by other phosphoinositides [Dove *et al.*, *Nature*, 1997, **390**, 187-192; Michell, *FEBS Journal*, 2013, **280**, 6281-6294]. Here we show that PtdIns(3,5)P₂ is structurally distinct from PtdIns(4,5)P₂ and other more common phospholipids, with unique physical chemistry. Using multiscale molecular dynamics techniques on the quantum level, single molecule, and in bilayer settings, we found that the negative charge of PtdIns(3,5)P₂ is spread over a larger area, compared to PtdIns(4,5)P₂, leading to a decreased ability to bind divalent ions. Additionally, our results match well with experimental data characterizing the cluster forming potential of these isomers in the presence of Ca²⁺ [Wang *et al.*, *Journal of the American Chemical Society*, 2012, **134**, 3387-3395; van den Bogaart *et al.*, *Nature*, 2011, **479**, 552-555]. Our results demonstrate that the different cellular roles of PtdIns(4,5)P₂ and PtdIns(3,5)P₂ *in vivo* are not simply determined by their localization by enzymes that produce or degrade them, but also by their molecular size, ability to chelate ions, and the partial dehydration of those ions, which might affect the ability of PtdIns(3,5)P₂ and PtdIns(4,5)P₂ to form phosphoinositide-rich clusters *in vitro* and *in vivo*.

1 Introduction

Polyphosphoinositides (PPIs) are a group of phospholipids present in eukaryotes that act as signaling molecules for a range of essential cellular processes. Defects in the synthesis, degradation, or localization of PPIs have been implicated in the acquisition of metastatic cell phenotypes, neurodegeneration, and other pathologies. Reversible phosphorylation of the hydroxyls on the inositol ring give rise to a family of PPIs, of which PtdIns(4,5)P₂ is the most common, that are distributed mainly on the cytoplasm-facing surfaces of membranes throughout the cell. Despite an abundance of less than 0.1% of all phosphoinositides, alterations in the synthesis of PtdIns(3,5)P₂, but not its more abundant isomer PtdIns(4,5)P₂, are associated with Charcot-Marie-Tooth dis-

ease, amyotrophic lateral sclerosis, and primary lateral sclerosis. Positioning of the phosphate groups on the inositol ring of PPIs appears to confer unique chemistry to each phosphoinositide that results in specific biological function.

The synthesis of PtdIns(3,5)P₂ and PtdIns(4,5)P₂ is catalyzed by different lipid metabolism pathways mediated by different enzymes. PtdIns(3,5)P₂ is generated exclusively from PtdIns(3)P via the zinc finger kinase PIKfyve in humans and rapidly dephosphorylated by an inositol polyphosphate 5-phosphatase to PtdIns(3)P or by myotubularin-related phosphatases to yield PtdIns(5)P¹. In contrast, PtdIns(4,5)P₂ can be created from PtdIns(4)P, PtdIns(5)P, or PtdIns(3,4,5)P₃ through kinases that use either the 4 or 5-hydroxyl as a substrate or a phosphatase that removes the 3-phosphate of PtdIns(3,4,5)P₃². Synthesis and turnover of these lipids is tightly controlled; although most eukaryotic cells produce only a very small amount of PtdIns(3,5)P₂, during hyperosmotic stress the concentration of PtdIns(3,5)P₂ increases twenty fold over a period of fifteen minutes with a concomitant drop in the level of PtdIns(3)P³⁻⁵. Whether PtdIns(3,5)P₂ is simply a read out for cellular stress or if its synthesis leads to changes in cellular membrane compartments is not known.

It is generally thought that the subcellular distribution of PtdIns(3,5)P₂ and PtdIns(4,5)P₂ is highly inhomogeneous

[†] Electronic Supplementary Information (ESI) available: Additional details on the computational and experimental methods. Additional supporting figures. See DOI: 10.1039/b000000x/

^a Institute for Medicine and Engineering, University of Pennsylvania, 1080 Vagelos Laboratories, 3340 Smith Walk, Philadelphia, PA, USA; E-mail: davids4@mail.med.upenn.edu

^b Department of Bioengineering, University of Pennsylvania, Philadelphia, PA, USA.

^c Department of Physiology, Perelman School of Medicine, University of Pennsylvania, Philadelphia, PA, USA.

and organelle specific, with PtdIns(4,5) P_2 primarily enriched on the cytoplasmic side of the plasma membrane and PtdIns(3,5) P_2 predominantly found in endosomal membranes and multivesicular bodies. It is experimentally very difficult to track the spatiotemporal dynamics of PtdIns(3,5) P_2 and PtdIns(4,5) P_2 *in vivo* because PPI sensors, including effector domains that have been identified as binding to PPIs *in vitro*, are only available and reliable for a few cases. Moreover, when such effectors are used to report the activity of PPIs in the cell, the question of whether effectors are recruited to the site of PPIs or if an excess of effectors can lead to production or localization of PPIs in a specific region is unanswered. PtdIns(3,5) P_2 and PtdIns(4,5) P_2 are responsible for orchestrating different cellular events, and it is unclear how specific protein effectors are targeted to very small quantities of PtdIns(3,5) P_2 or PtdIns(4,5) P_2 . Failure to distinguish between polyphosphoinositide isomers has generally led to opposing observations and conflicting reports in intracellular trafficking. Recognizing the importance of the differences in isomers continues to lead to the discovery of new trafficking mechanisms, as evidenced by the recent discovery of a clathrin-independent pathway for endocytosis regulated specifically by PtdIns(3,4) P_2 ⁶.

Either in simple systems *in vitro* or in the physiological environment of the cell, it is very difficult to isolate the effects of membrane crowding, electrostatic interactions, pH, and varying ionic conditions. Our results are able to address these aspects of PPI structure and function through molecular dynamics (MD) simulations of isolated PtdIns(3,5) P_2 and PtdIns(4,5) P_2 molecules and bilayers containing PtdIns(3,5) P_2 and PtdIns(4,5) P_2 . In this paper, we show that PtdIns(4,5) P_2 is a dynamic molecule, changing the orientation and size of its head group in response to ion fluxes, in addition to known changes of its protonation state, which leads to dehydration of the membrane interface where it is present. These features of PtdIns(4,5) P_2 make it a good candidate to participate in the formation of endocytic pits and clathrin-coated vesicles where the membrane is highly curved and there is attachment to the cytoskeleton⁷. In contrast, PtdIns(3,5) P_2 is much larger, does not distinguish significantly between divalent cations, and has no known stereospecific adapter proteins that bind it but not PtdIns(4,5) P_2 . Under hyperosmotic stress, there is increased production of PtdIns(3,5) P_2 in the trans-Golgi network, leading to enlargement of multivesicular bodies (and vacuoles in yeast), which based on our studies, could depend on the large size and distributed negative charge of PtdIns(3,5) P_2 which alter the membrane potential and likely increase the stiffness through the accumulation of an electrical double layer around these vesicles.

It is intriguing that our results show a reversal in preference for Ca^{2+} versus Mg^{2+} binding between PtdIns(4,5) P_2 , which

we predict to prefer Ca^{2+} , and PtdIns(3,5) P_2 , which we predict to prefer Mg^{2+} . Such a change in preference can have significant implications for how PPIs are able to differentially recruit binding proteins depending on the relative abundance of Ca^{2+} versus Mg^{2+} in a specific cell at a given instant of time.

2 Results and discussion

2.1 PtdIns(3,5) P_2 adopts a different structural geometry than PtdIns(4,5) P_2

Figure 1 shows the structural differences between two PPI isomers, PtdIns(3,5) P_2 and PtdIns(4,5) P_2 , computed using electronic structure calculations and hybrid quantum mechanics/molecular mechanics (QM/MM) simulations of a single PPI isomer in a water sphere with counterions (Figure 1 in ESI[†]). The head group of PtdIns(3,5) P_2 has a much larger extent, compared to PtdIns(4,5) P_2 , as judged by the spread of the inositol phosphate oxygens. A fundamental feature of PtdIns(3,5) P_2 is its large size; at 95 Å² it is significantly larger than other phospholipids in the cell. The angle the head group makes with the acyl chains (head-tail angle) is affected by monovalent and divalent ions. The addition of Ca^{2+} or Mg^{2+} to either isomer tends to increase the head-tail angle, causing the phospholipid head group to extend away from the plane of the bilayer. Notably, Ca^{2+} has a much stronger effect on PtdIns(4,5) P_2 than on PtdIns(3,5) P_2 , likely owing to its tight coordination between the two vicinal phosphate groups of PtdIns(4,5) P_2 that does not occur with PtdIns(3,5) P_2 . The inability of PtdIns(3,5) P_2 to chelate divalent cations as well leads to repulsion between the like-charged phosphomonoester groups, giving rise to its large spread area. K^+ increases the head-tail angle slightly more than Na^+ and the head-tail distribution angle distribution of PtdIns(4,5) P_2 with Na^+ is best fit by the sum of two Gaussian distributions (Figure 2 in ESI[†]). The structure of PtdIns(4,5) P_2 is more variable than PtdIns(3,5) P_2 , becoming more compact laterally and extended vertically, in response to Ca^{2+} . Other lipids that also bind Ca^{2+} , such as phosphatidylserine, do not alter their structure in this manner⁷.

2.2 PtdIns(3,5) P_2 prefers to be protonated on the 5-phosphate group

Although most lipids in the cell are zwitterionic or neutral, some are highly anionic. A large negative charge density on such lipids is associated with their ability to bind proteins with a specific arrangement of basic residues and, in the absence of neutralizing proteins, sets up a cloud of counterions in the adjacent cytosol. In the case of PtdIns(3,5) P_2 and PtdIns(4,5) P_2 we set out to establish the distribution of nega-

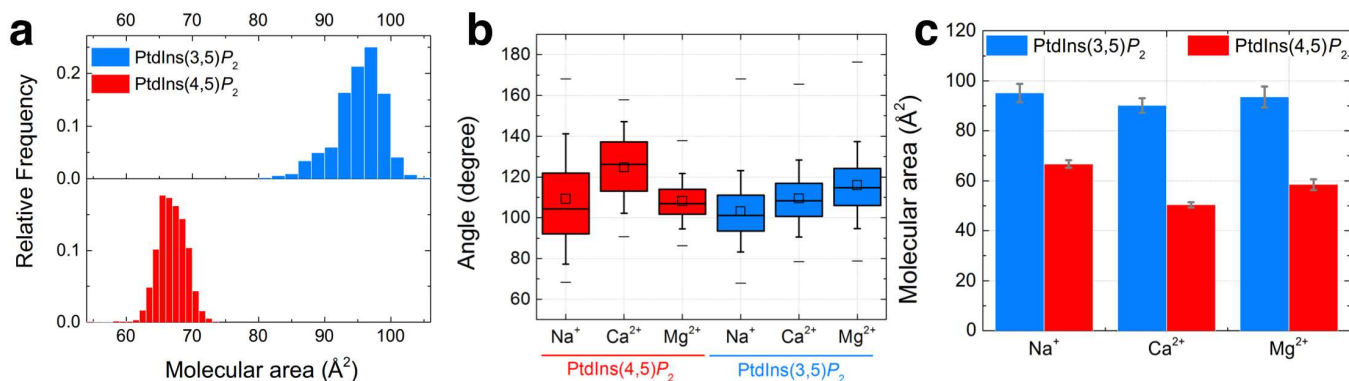


Fig. 1 The molecular area and the angle formed between the head group of PtdIns(3,5) P_2 or PtdIns(4,5) P_2 with the acyl chains. a, A comparison of the molecular area of a single molecule of PtdIns(3,5) P_2 or PtdIns(4,5) P_2 in the presence of neutralizing Na^+ . b, The distribution of head-tail angle for PtdIns(3,5) P_2 or PtdIns(4,5) P_2 in the presence of monovalent and divalent cations. The distributions can be characterized by a single Gaussian curve in most cases; 180° corresponds to the head group extending parallel to the acyl chains and 90° corresponds to the head group being normal to the acyl chains (i.e., lying flat along a hypothetical bilayer). Bars represent the 25th and 75th percentiles of the distributions and dashes mark the range of the distributions. c, The effect of monovalent and divalent cations on the molecular area of PtdIns(3,5) P_2 or PtdIns(4,5) P_2 . Divalent ions strongly affect the molecular area of PtdIns(4,5) P_2 but not PtdIns(3,5) P_2 . Bars represent the standard deviation of the distributions.

tive charge on head groups of PtdIns(3,5) P_2 and PtdIns(4,5) P_2 to determine the protonation state and separation of their phosphate groups. Umbrella sampling was used to determine the potential of mean force (PMF) for protonation at either the 3 or the 5-phosphate group on the inositol ring, maintaining a net molecular charge of -4 for PtdIns(3,5) P_2 ⁸. Protonation of the 3-phosphate group is 4 kcal/mol less stable than protonation of the 5-phosphate group, and about 10 kcal/mol less stable than two protons shared between the 3-phosphate, 4-hydroxyl, and 5-phosphate (Figure 2a-c). This intermediate form of proton sharing is consistent with NMR reports of the the 3-phosphate and 5-phosphate carrying charges of -1.52 and -1.73 , respectively⁸. Although the final state is a relatively stable configuration that will not relax to the starting configuration after constraints are released, it is not the preferred geometry for PtdIns(3,5) P_2 (Figure 2c, inset). The preferred geometry for PtdIns(3,5) P_2 is a twist chair form of the inositol sugar ring, as the 2-hydroxyl group is pulled out of its axial plane towards the 3-phosphate ester oxygen (Figure 3 in ESI[†]) that is not seen with PtdIns(4,5) P_2 or in biological crystal structures with inositol.

Protonation of the 4-phosphate over the 5-phosphate of PtdIns(4,5) P_2 is less favorable by 20 kcal/mol (Figure 2d-f). The final structure of this calculation shows protonation of an ester oxygen that is not stable when constraints are released, but total proton dissociation from the 5-phosphate of PtdIns(4,5) P_2 can be achieved with additional constraints, generating a hydronium ion and increasing the charge of the phospholipid to -5 ⁹. The charge of PtdIns(4,5) P_2 directly modulates its ability to form clusters in numerical simulations,

and in experiments, the pH of the fluid buffer in contact with the membrane acts in the same way^{8,10}. Other lipids, such as phosphatidic acid, have been proposed to alter their binding to cellular effectors based on pH near the plasma membrane^{11,12}. The charge of PtdIns(4,5) P_2 is likely modulated by the pH and ionic environment at the plasma membrane resulting from intracellular ion fluxes, mediating its ability to form hydrogen bonds with other PPIs or bind to proteins containing effector modules. The charge of PtdIns(3,5) P_2 is more evenly distributed across its head group and it cannot be coordinated as specifically by proteins that contain PPI-binding domains.

2.3 PtdIns(3,5) P_2 reacts to divalent cations less strongly than PtdIns(4,5) P_2

Cytoplasmic divalent cations, such as magnesium (Mg^{2+}) and calcium (Ca^{2+}), are capable of reducing the molecular area of both PtdIns(3,5) P_2 and PtdIns(4,5) P_2 principally by decreasing the distance between their respective phosphomonoester groups. Ca^{2+} binds tightly to PtdIns(4,5) P_2 with a dissociation constant on the order of $4.6 \mu\text{M}$ and generally outcompetes Mg^{2+} when present at the same concentration¹³.

In simulations where divalent ions are free to interact with a single phosphoinositide (see Figure 1 for system setup in ESI[†]), Ca^{2+} prefers to bind closer to PtdIns(3,5) P_2 than Mg^{2+} (Figure 3a) and the PMF for PtdIns(3,5) P_2 binding to Ca^{2+} and Mg^{2+} has been calculated using umbrella sampling¹⁴ (Figure 3b-d). Both divalent ions localize to the 3-phosphate, which carries a more negative charge density, and the PMF curves follow a similar trend. Notably, Mg^{2+} , which is more

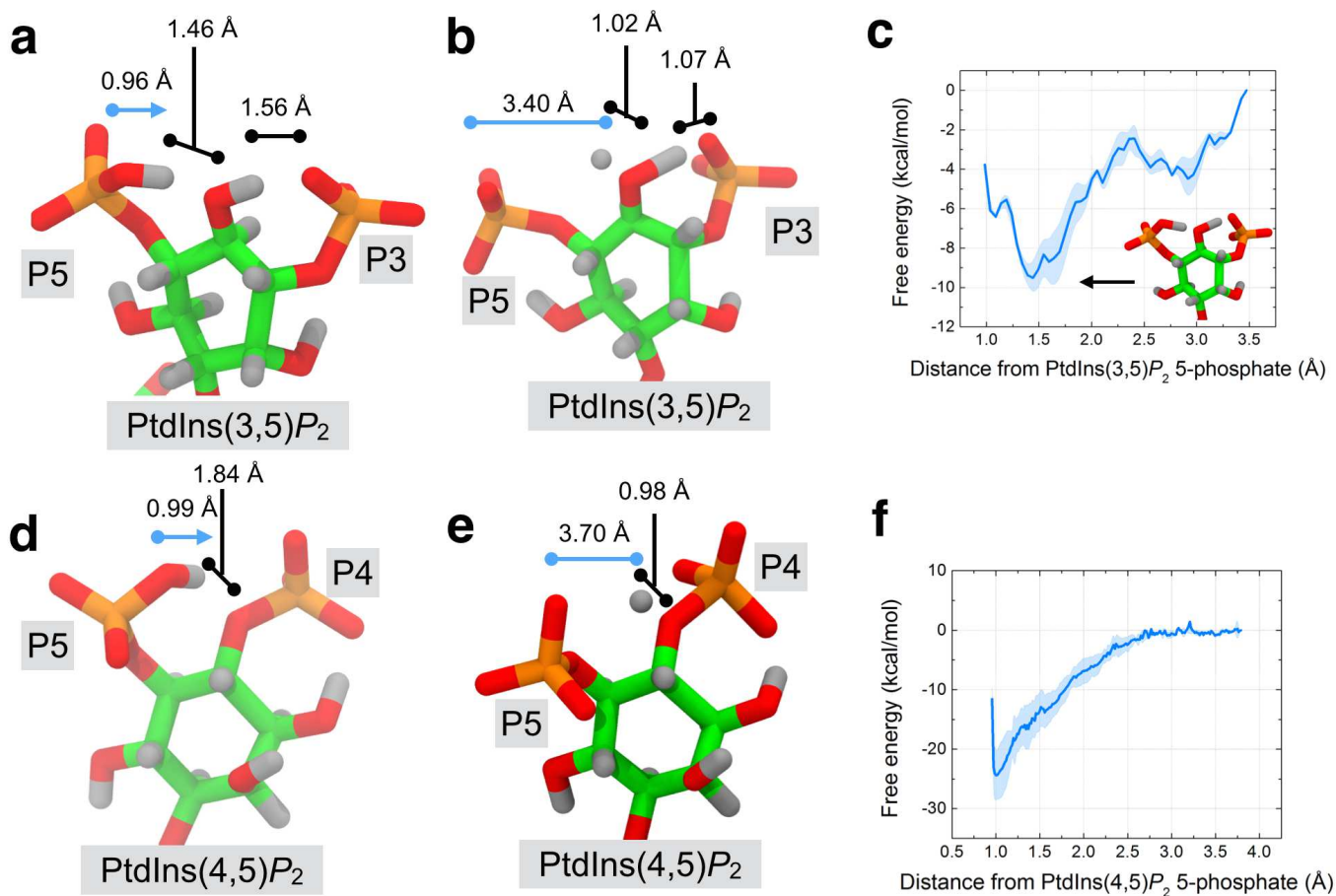


Fig. 2 The free energy for removing a proton from the 5-phosphate group of PtdIns(3,5)P₂ or PtdIns(4,5)P₂. a, A stable initial configuration to test for protonation on the 3 (P3) and 5-phosphate (P5) of PtdIns(3,5)P₂. The umbrella sampling (US) reaction coordinate is marked by the blue arrow. b, The final configuration of US resulting in a proton moving from the 5-phosphate to the 4 hydroxyl and a proton moving from the 4 hydroxyl to the 3-phosphate. Surrounding waters are not shown for clarity. c, The potential of mean force (PMF) from state a to state b. d, A stable initial configuration to test for protonation on the 4 (P4) and 5-phosphate (P5) groups of PtdIns(4,5)P₂ after an *ab initio* electronic structure optimization, and e, the final configuration of US. f, The PMF corresponding to proton dissociation from the 5-phosphate group of PtdIns(4,5)P₂ and binding to the 4-phosphate ester oxygen. The blue line segments with an arrowhead show the direction of pulling and initial reaction coordinate; the blue line segments (no arrowhead) show the final reaction coordinate distance.

difficult to dehydrate despite its smaller hydration shell even in classical force fields, is strongly disfavored from binding between the 3 and 5-phosphate groups (Figure 3c). Ca^{2+} binding to both $\text{PtdIns}(3,5)\text{P}_2$ and $\text{PtdIns}(4,5)\text{P}_2$ is favorable; it is almost an order of magnitude more favorable binding to the latter owing to the stripping of an additional water from the Ca^{2+} solvation shell (Figure 3d). These data suggest that the binding of Ca^{2+} might act as a switch that regulates a transition between two structural forms of $\text{PtdIns}(4,5)\text{P}_2$; one form may be found distributed throughout the plasma membrane and constitutively bound to proteins, such as those that contain a phosphoinositide-specific PH domain and bind with μM to mM affinity^{15,16}, and the other form localized to specific regions of high curvature, such as during exocytosis, mediating Ca^{2+} -triggered secretion of vesicles^{7,17}.

In bulk water, Ca^{2+} and Mg^{2+} are both solvated by a little more than six waters on average, although the solvation radius around Mg^{2+} is 2.28 Å compared to 2.60 Å for Ca^{2+} (Figure 3e, refer to Methods section). When bound to $\text{PtdIns}(3,5)\text{P}_2$, a phosphate oxygen atom replaces one water oxygen (Figure 3f-g). When Ca^{2+} and Mg^{2+} bind to $\text{PtdIns}(4,5)\text{P}_2$, Ca^{2+} is much more strongly bound, and two phosphate oxygen atoms replace two water oxygens in the solvent shell (Figure 3h). In this case, the electrostatic attraction is so great that even stripping the first water from the hydration shell around 6 Å is not significantly unfavorable.

2.4 $\text{PtdIns}(3,5)\text{P}_2$ alters bilayer properties distinctly from $\text{PtdIns}(4,5)\text{P}_2$

The increased area and decreased charge density of $\text{PtdIns}(3,5)\text{P}_2$ affect the properties of a phospholipid bilayer in unique ways. In a bilayer simulations with other phospholipids, as shown in single molecule simulations, the molecular area of $\text{PtdIns}(3,5)\text{P}_2$ with either Ca^{2+} or Mg^{2+} is extremely large, whereas the molecular area of $\text{PtdIns}(4,5)\text{P}_2$ with these ions is significantly smaller. Simulating these lipids in a bilayer context (Figure 4a) reveals a subpopulation of $\text{PtdIns}(4,5)\text{P}_2$ with bound Mg^{2+} that is smaller than expected from single molecule simulations. As the PMF for Mg^{2+} binding to $\text{PtdIns}(4,5)\text{P}_2$ contains a broad minimum between 3 and 9 Å, there may be several stable configurations of the head group.

The distance between the divalent cations and the plane of the membrane, judged here as the plane containing the phosphodiester phosphorus atom of the lipids, can be computed directly. In contrast to the other ion and lipid combinations, there is a significant proportion of Ca^{2+} counterions bound within 4 Å of the phosphodiester group of $\text{PtdIns}(4,5)\text{P}_2$ and more Ca^{2+} binds to either phosphomonoester group (i.e., 8 to 12 Å from the phosphodiester) of $\text{PtdIns}(4,5)\text{P}_2$ (Figure 4b) than either ion binds to $\text{PtdIns}(3,5)\text{P}_2$ or Mg^{2+} binding

to $\text{PtdIns}(4,5)\text{P}_2$. The hydration shells for Ca^{2+} and Mg^{2+} in the bilayer system (using the same force field) reveal a more complicated dynamic than the single molecule simulations (Figure 4d). Unlike the single molecule systems, where Mg^{2+} and Ca^{2+} had distinct hydrated radii, Ca^{2+} binding to $\text{PtdIns}(3,5)\text{P}_2$ in a bilayer showed an additional, dominant peak at the Mg^{2+} hydrated radius. These data are consistent with the PMF in Figure 3b that shows Ca^{2+} and Mg^{2+} may be almost indistinguishable to $\text{PtdIns}(3,5)\text{P}_2$ yet very different to $\text{PtdIns}(4,5)\text{P}_2$. The increase in molecular area between $\text{PtdIns}(3,5)\text{P}_2$ and $\text{PtdIns}(4,5)\text{P}_2$ as well as the difference in ion dehydration is not accompanied by a difference in head-tail angle (Figure 4e).

Packing in the membrane, and attractive intermolecular hydrogen bonding between lipids, affects the availability of the 3, 4, and 5-phosphate groups to interact with mobile counterions. Snapshots of the simulations reveal several binding sites for the divalent ions (Figure 4 in ESI[†]), such as bridging two phospholipids via their phosphodiester groups or binding exclusively to a single $\text{PtdIns}(4,5)\text{P}_2$ in a pair. Clusters containing a high percentage of $\text{PtdIns}(4,5)\text{P}_2$ have been imaged in PC12 cells¹⁸; the unique interaction between Ca^{2+} and $\text{PtdIns}(4,5)\text{P}_2$ could explain how the concentration of $\text{PtdIns}(4,5)\text{P}_2$ increases to hundreds of times its bulk value in those regions without requiring localized production or decreased phosphatase activity. The two PPI isomers have similar affinities for Ca^{2+} , but as seen in Figure 4f, different capacities to form nanoscale clusters. Ca^{2+} and Mg^{2+} are able to induce cluster formation in Langmuir monolayers containing PPIs. Whereas the clusters formed in the presence of 1 μM Ca^{2+} are larger and more round, the clusters formed by 2 mM Mg^{2+} are smaller with irregular boundaries¹⁹. The clusters formed by the addition of 1 μM Ca^{2+} to 25% $\text{PtdIns}(4,5)\text{P}_2$ are 80 nm in diameter and match observations of $\text{PtdIns}(4,5)\text{P}_2$ clusters in the cell using other methods^{18,20}. In contrast, clusters formed by the addition of Ca^{2+} to 25% $\text{PtdIns}(3,5)\text{P}_2$ are smaller, with more diverse shapes, and more similar to clusters formed with Mg^{2+} . That simulations reveal similar binding energies for Ca^{2+} and Mg^{2+} to $\text{PtdIns}(3,5)\text{P}_2$ and very different binding energies for $\text{PtdIns}(4,5)\text{P}_2$ supports these observations.

3 Conclusions

In addition to its important role in human neurodevelopment, the proper amount and sub-cellular localization of $\text{PtdIns}(3,5)\text{P}_2$ is essential for membrane trafficking events^{21,22}. In this paper, we show that the chemical structure of $\text{PtdIns}(3,5)\text{P}_2$ lends it distinct physical properties from the more common polyphosphoinositide isomer, $\text{PtdIns}(4,5)\text{P}_2$, and these effects are manifest in membranes that contain $\text{PtdIns}(3,5)\text{P}_2$. Specifically, $\text{PtdIns}(3,5)\text{P}_2$ has a more dif-

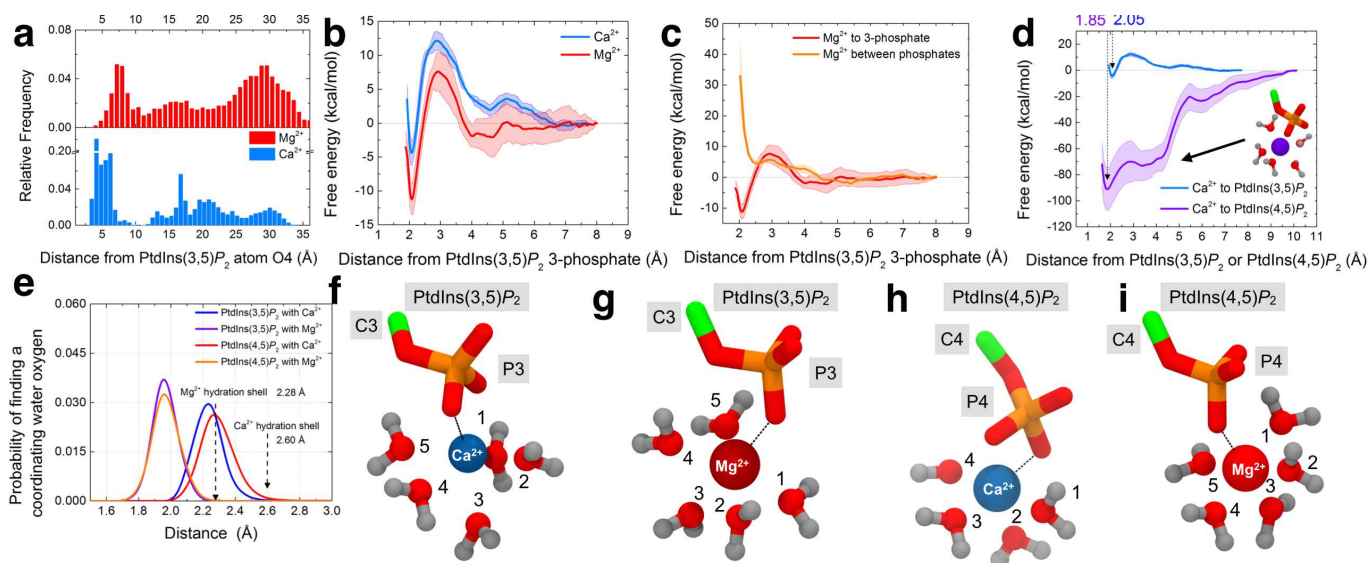


Fig. 3 The divalent ion binding characteristics of PtdIns(3,5) P_2 and PtdIns(4,5) P_2 . a, The unbiased distribution of divalent ion distances to PtdIns(3,5) P_2 . b, The potential of mean force for divalent ion binding to PtdIns(3,5) P_2 . c, A comparison of the potentials of mean force for Mg^{2+} to bind to the 3-phosphate only or between the two phosphate groups of PtdIns(3,5) P_2 . d, A comparison of the potentials of mean force for Ca^{2+} to bind to either PtdIns(3,5) P_2 or PtdIns(4,5) P_2 ; the minima at 1.85 Å and 2.05 Å corresponding to panels h and f respectively, whereas a metastable state where Ca^{2+} is 4.0 Å from PtdIns(4,5) P_2 , with five coordinating waters, is shown in the inset. e, The first hydration shells of Mg^{2+} with PtdIns(3,5) P_2 (g) or PtdIns(4,5) P_2 (i) and Ca^{2+} with PtdIns(3,5) P_2 (f) or PtdIns(4,5) P_2 (h).

fuse negative charge distributed across its head group, is much larger, binds less tightly to divalent ions, and has a lower potential to form clusters in mixed membranes.

Several proteins bind to both divalent ions and PPIs with dissociation constants in the range of μM to mM , such as synaptotagmin-1, the main effector protein for neural exocytosis²³; gelsolin, a protein that binds to actin and couples the cytoskeleton to the plasma membrane²⁴; and phospholipase C, the enzyme responsible for cleaving PtdIns(4,5) P_2 and PtdIns(3,5) P_2 leading to the generation of second messengers and regulation of myriad cell processes^{25,26}. Proteins that contain a C2 domain, such as protein kinase C, use PtdIns(4,5) P_2 and Ca^{2+} cooperatively to coordinate association of the protein with the plasma membrane²⁶. The two C2 domains of rabphilin-3A differ in their affinity for Ca^{2+} and reports have noted that Ca^{2+} increases the affinity of such domains for PtdIns(4,5) P_2 as well^{27,28}. There is little structural difference between the C2 domain of protein kinase C alpha crystallized with and without both phosphatidylserine and Ca^{2+} , suggesting that counterion-induced protein-reorganization is not responsible for the increased affinity of charged lipids in the presence of divalent ions (Figure 5 in ESI[†]). Moreover, two Ca^{2+} ions mediate the interaction of phosphatidylserine with seven amino acids in the protein, so this effect seems distinct from simple charge neutralization. These data show that divalent ions have the ability to mediate the interactions between

PPIs and their protein binding partners in biological systems.

It has been known for almost two decades that sub- mM levels of Ca^{2+} can alter the morphology of mixed vesicles containing phosphatidylcholine and PtdIns(4,5) P_2 ²⁹. A more recent study has characterized the differential effects of Ca^{2+} and Mg^{2+} on the two phosphomonoester groups of PtdIns(4,5) P_2 , highlighting that Ca^{2+} has a stronger effect on either phosphomonoester group compared to Mg^{2+} ³⁰. Our results describe the mechanism through which divalent ions exert their effects on PPIs, the difference between Ca^{2+} and Mg^{2+} , and why PtdIns(4,5) P_2 is more strongly affected by Ca^{2+} than PtdIns(3,5) P_2 . We show that the absence of vicinal phosphates confers unique chemistry to PtdIns(3,5) P_2 , providing evidence for why proteins that stereospecifically bind PtdIns(4,5) P_2 do not recognize PtdIns(3,5) P_2 as well, and suggest the biological role of PtdIns(3,5) P_2 might be exerted through changes in the physical properties of membranes rather than specific binding.

4 Methods

Single molecule MD simulations were carried out in the Number, Volume, Temperature (NVT) ensemble using Langevin dynamics at 300 K with the CHARMM C36 force field for lipids^{31–33} and the CHARMM program^{34,35}. The single PPI isomer was centered in a TIP3P water sphere approximately 40

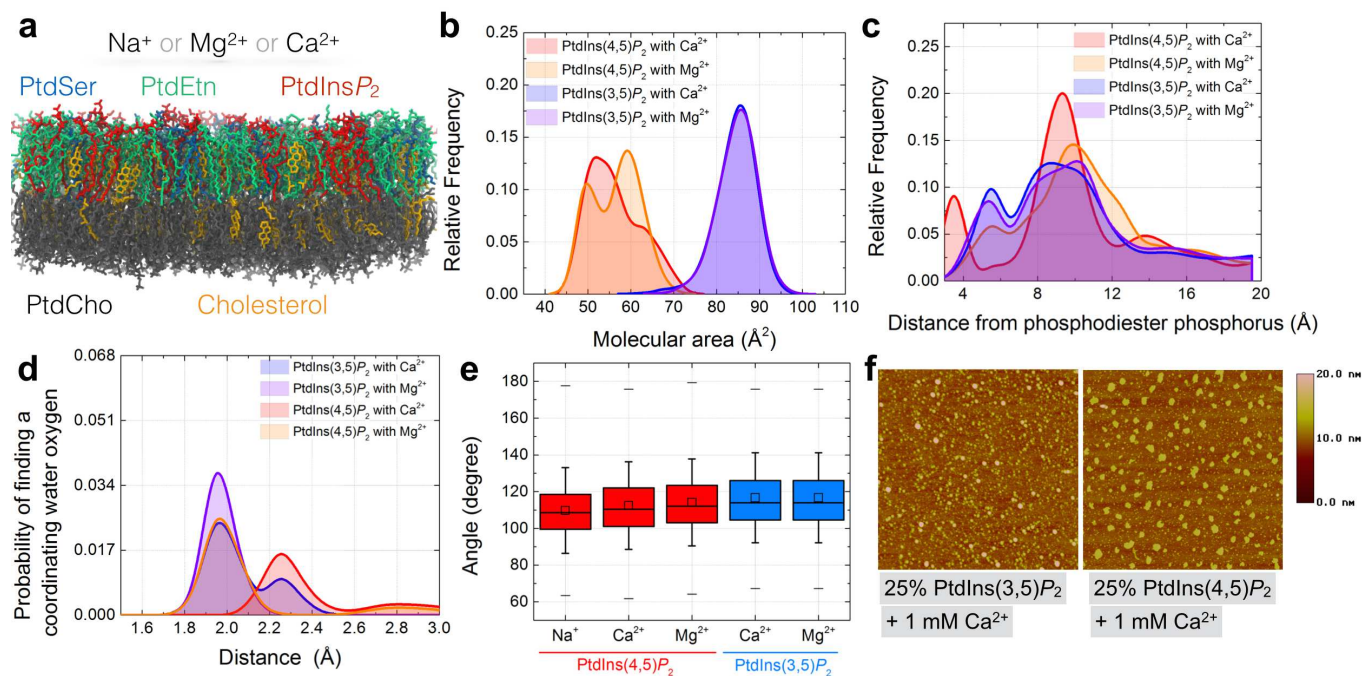


Fig. 4 The molecular area and ion binding characteristics of PtdIns(3,5) P_2 or PtdIns(4,5) P_2 when embedded in a membrane system in silico or a monolayer in vitro. a, A schematic of the bilayer simulation system showing the various lipid components. b, The distribution of molecular areas for PtdIns(3,5) P_2 and PtdIns(4,5) P_2 with divalent ions in a bilayer containing other neutral lipids (upper leaflet: 75% PtdCho, 25% cholesterol; lower leaflet: 50% PtdEtn, 25% cholesterol, 15% PtdSer, 10% PtdIns(4,5) P_2 or PtdIns(3,5) P_2). c, The distribution of distances between the divalent ions and the lipids. d, The hydration shell of Ca^{2+} and Mg^{2+} in the bilayer simulations. e, The angle made between the head group of PPI isomers and the acyl chains. f, Experimental cluster formation in monolayers containing PtdIns(3,5) P_2 or PtdIns(4,5) P_2 in the presence of Ca^{2+} .

Å in diameter (Figure 1 in ESI[†]). The waters on the edge were held fixed to prevent the sphere from expanding during the course of the simulation. Na⁺, Ca²⁺, or Mg²⁺ were added to neutralize the −4 charge of the singly protonated PPI; to investigate lipid-ion binding, a single ion was permitted to interact with a single lipid. Head-tail angle was assessed using atoms C2, P, C4 for residue type SAPI with appropriate patches in the C36 force field. Molecular area was computed by tracking the maximum distance between the six phosphomonoester oxygen atoms and squaring the result to generate the smallest two-dimensional box that a given lipid could occupy.

The PMFs in Figure 2 were completed using hybrid QM/MM MD simulations. The system was split into two quantum regions: QM1, containing only phospholipid atoms, and QM2, containing water and ions (if present). Two single link atoms connect the QM regions to classical regions, as described in Slochower *et al.*⁹. The first link atom was placed between the third and fourth carbon of the inositol ring for PtdIns(4,5)P₂ or between the second and third carbon of the inositol ring for PtdIns(3,5)P₂, the second link atom was placed between the fifth and sixth carbon of the inositol ring for either PPI. QM2 typically contains the five or six closest interacting waters and a divalent ion (if present). We performed these calculations using a combination of GAMESS-UK³⁶ and CHARMM. Both QM regions (36–40 atoms) were treated with density functional theory (DFT) using the hybrid functional B3LYP/6-31G; this basis set was shown to be sufficient for treating PtdIns(4,5)P₂-ion interactions in our previous work Slochower *et al.*⁹.

In the QM/MM simulations, we performed the usual energy minimization (5000 steepest descent followed by 5000 steps of adopted basis Newton-Raphson) and constant temperature equilibration using Langevin dynamics at 300 K using a piston frequency of 10 ps^{−1} before standard procedures for pure MM systems using a 1 fs time step of integration. The QM/MM simulations were run for a total of 5 or 10 ps. To compare the protonation states of the inositol phosphate groups of the two PPI isomers, the ions added to neutralize the negative charge of the isomers were kept fixed to prevent undesired interactions during umbrella sampling.

The PMFs in Figure 2 were calculated using a reaction coordinate biasing the hydrogen atom from one or more phosphomonoester oxygen atoms. The PMFs were computed from a series of US windows spaced 0.2 Å or closer, with additional sampling windows added as needed to ensure overlap. Initial coordinates for each US window were taken from short equilibration simulations at the target distance. The US simulations were analyzed with the weighted histogram analysis method¹⁴. The PMFs in Figure 3 were completed using classical all-atom MD simulations. The same water sphere, umbrella sampling window spacing, and analysis methods described for the QM/MM calculations were employed. These

PMFs used a reaction coordinate biasing the divalent metal ion from the oxygen atom it was found to bind in unbiased simulations on the 3 or 4-phosphate group of PtdIns(3,5)P₂ or PtdIns(4,5)P₂, respectively.

The simulations in Figure 4 were carried out using the CHARMM C36 force field for lipids incorporating a pre-patched version of PtdIns(4,5)P₂ and PtdIns(3,5)P₂ in the Gromacs 4.5 program³⁷. Phospholipids and cholesterol were randomly distributed on a grid (400 total lipids and cholesterol molecules per monolayer; 800 total lipids and cholesterol molecules per system) and equilibrated for 20 ns before analysis of the production runs. The Number, Pressure, Temperature (NPT) ensemble was used with cubic periodic boundary conditions, real space electrostatics cut off at 12 Å and a smooth switching distance of 10 Å, particle mesh Ewald (PME) summation grid spacing of 1 Å, non-bonded interaction pair list distance of 13.5 Å, MD time step of 2.0 fs, temperature control by Langevin dynamics at 310 K with a damping coefficient of 5 ps^{−1}, and pressure coupling using the semi-isotropic Parinello-Rahman algorithm with a 2.0 ps time constant, reference pressure of 1.0 bar, and compressibility of 4.5 × 10^{−5} bar^{−1}. Total simulation time per system was approximately 100 ns.

Supported lipid monolayers containing 75% 1-stearoyl-2-oleoyl-phosphatidylcholine and 25% 1,2-dioleoyl-PtdIns(3,5)P₂ or 1,2-dioleoyl-PtdIns(4,5)P₂ were prepared by transferring monolayers compressed to 20 mN/m on a buffered subphase of 10 mM HEPES, 1 μM EDTA and 5 mM DTT, pH 7.4 with or without addition of divalent cations, from a Langmuir trough (Kibron, Inc. Helsinki FI) onto glass coverslips using the Langmuir-Schaeffer method. AFM images of air-dried supported lipid monolayers were made using tapping mode AFM (Digital Instruments, Santa Barbara, CA) and processed by Nanoscope(R) IIIa software (v. 5.12; Digital Instruments) as previously described¹³.

5 Acknowledgements

The authors thank Ryan Bradley for assistance in designing and running the bilayer simulations.

This work was supported in part by grants from the National Science Foundation (DMR-1120901) and the USPHS (NIDDK R01 DK083592, NIH U01-EB016027, and T32 HL007954). The research leading to these results has received funding from the European Commission grant FP7-ICT-2011-9-600841. Computational resources were provided in part by the National Partnership for Advanced Computational Infrastructure under grant MCB060006 from XSEDE.

References

- 1 R. H. Mitchell and S. K. Dove, *EMBO J.*, 2009, **28**, 86–87.

- 2 M. Vicinanza, G. D'Angelo, A. Di Campli and M. A. De Matteis, *EMBO J.*, 2008, **27**, 2457–2470.
- 3 S. K. Dove, F. T. Cooke, M. R. Douglas, L. G. Sayers, P. J. Parker and R. H. Michell, *Nature*, 1997, **390**, 187–192.
- 4 R. H. Michell, *FEBS J.*, 2013, **280**, 6281–6294.
- 5 A. J. McCartney, Y. Zhang and L. S. Weisman, *Bioessays*, 2014, **36**, 52–64.
- 6 E. Boucrot, A. P. A. Ferreira, L. Almeida-Souza, S. Debard, Y. Vallis, G. Howard, L. Bertot, N. Sauvonnet and H. T. McMahon, *Nature*, 2015, **517**, 460–465.
- 7 M. Hu, J. J. Briguglio and M. Deserno, *Biophysical Journal*, 2012, **102**, 1403–1410.
- 8 E. E. Kooijman, K. E. King, M. Gangoda and A. Gericke, *Biochemistry*, 2009, **48**, 9360–9371.
- 9 D. R. Slochowar, P. J. Huwe, R. Radhakrishnan and P. A. Janmey, *The Journal of Physical Chemistry B*, 2013, **117**, 8322–8329.
- 10 W. G. Ellenbroek, Y. H. Wang, D. A. Christian, D. E. Discher, P. A. Janmey and A. J. Liu, *Biophysical Journal*, 2011, **101**, 2178–2184.
- 11 S. Loew, E. E. Kooijman and S. May, *Chemistry and Physics of Lipids*, 2013, **169**, 9–18.
- 12 W. J. Wang, N. A. Anderson, A. Travesset and D. Vaknin, *The Journal of Physical Chemistry B*, 2012, **116**, 7213–7220.
- 13 Y.-H. Wang, A. Collins, L. Guo, K. B. Smith-Dupont, F. Gai, T. Svitkina and P. A. Janmey, *Journal of the American Chemical Society*, 2012, **134**, 3387–3395.
- 14 B. Roux, *Computer Physics Communications*, 1995, **91**, 275–282.
- 15 M. A. Lemmon, K. M. Ferguson, R. O'Brien, P. B. Sigler and J. Schlessinger, *Proceedings of the National Academy of Sciences of the United States of America*, 1995, **92**, 10472–10476.
- 16 S. Shenoy, P. Shekhar, F. Heinrich, M. C. Daou, A. Gericke, A. H. Ross and M. Lösche, *PLoS one*, 2012, **7**, e32591.
- 17 G. Di Paolo and P. De Camilli, *Nature*, 2006, **443**, 651–657.
- 18 G. van den Bogaart, K. Meyenberg, H. J. Risselada, H. Amin, K. I. Willig, B. E. Hubrich, M. Dier, S. W. Hell, H. Grubmüller, U. Diederichsen and R. Jahn, *Nature*, 2011, **479**, 552–555.
- 19 D. R. Slochowar, Y.-H. Wang, R. W. Tourdot, R. Radhakrishnan and P. A. Janmey, *Advances in colloid and interface science*, 2014.
- 20 J. Wang and D. A. Richards, *Biology open*, 2012, **1**, 857–862.
- 21 A. S. Nicot and J. Laporte, *Traffic*, 2008, **9**, 1240–1249.
- 22 S. K. Dove, K. Dong, T. Kobayashi, F. K. Williams and R. H. Michell, *Biochemical Journal*, 2009, **419**, 1–13.
- 23 G. van den Bogaart, K. Meyenberg, U. Diederichsen and R. Jahn, *The Journal of Biological Chemistry*, 2012, **287**, 16447–16453.
- 24 K. M. K. Lin, E. E. Wenegieme, P. J. P. Lu, C. S. C. Chen and H. L. H. Yin, *The Journal of Biological Chemistry*, 1997, **272**, 20443–20450.
- 25 S. Thore, A. Wuttke and A. Tengholm, *Diabetes*, 2007, **56**, 818–826.
- 26 J. Guillén, C. Ferrer-Orta, M. Buxaderas, D. Pérez-Sánchez, M. Guerrero-Valero, G. Luengo-Gil, J. Pous, P. Guerra, J. C. Gómez-Fernández, N. Verdager and S. Corbalán-García, *Proceedings of the National Academy of Sciences of the United States of America*, 2013, **110**, 20503–20508.
- 27 S. H. Chung, W. J. Song, K. Kim, J. J. Bednarski, J. Chen, G. D. Prestwich and R. W. Holz, *The Journal of Biological Chemistry*, 1998, **273**, 10240–10248.
- 28 P. Montaville, N. Coudeville, A. Radhakrishnan, A. Leonov, M. Zweckstetter and S. Becker, *Protein science : a publication of the Protein Society*, 2008, **17**, 1025–1034.
- 29 L. a. Flanagan, C. C. Cunningham, J. Chen and G. D. Prestwich, *Biophysical Journal*, 1997.
- 30 Z. T. Graber, A. Gericke and E. E. Kooijman, *Chemistry and Physics of Lipids*, 2014, **182**, 62–72.
- 31 J. B. Klauda, R. M. Venable, J. A. Freites, J. W. O'Connor, D. J. Tobias, C. Mondragon-Ramirez, I. Vorobyov, A. D. MacKerell and R. W. Pastor, *The Journal of Physical Chemistry B*, 2010, **114**, 7830–7843.
- 32 R. W. Pastor and A. D. MacKerell, *The Journal of Physical Chemistry Letters*, 2011, **2**, 1526–1532.
- 33 E. R. Hatcher, O. Guvench and A. D. MacKerell Jr., *Journal of chemical theory and computation*, 2009, **5**, 1315–1327.
- 34 B. R. Brooks, C. L. Brooks, A. D. MacKerell, L. Nilsson, R. J. Petrella, B. Roux, Y. Won, G. Archontis, C. Bartels, S. Boresch, A. Caffisch, L. Caves, Q. Cui, A. R. Dinner, M. Feig, S. Fischer, J. Gao, M. Hodoscek, W. Im, K. Kuczera, T. Lazaridis, J. Ma, V. Ovchinnikov, E. Paci, R. W. Pastor, C. B. Post, J. Z. Pu, M. Schaefer, B. Tidor, R. M. Venable, H. L. Woodcock, X. Wu, W. Yang, D. M. York and M. Karplus, *Journal of Computational Chemistry*, 2009, **30**, 1545–1614.
- 35 B. R. Brooks, R. E. Bruccoleri, B. D. Olafson, D. J. States, S. Swaminathan and M. Karplus, *Journal of Computational Chemistry*, 1983, **4**, 187–217.
- 36 M. F. Guest, I. J. Bush, H. Van Dam, P. Sherwood, J. Thomas, J. H. Van Lenthe, R. Havenith and J. Kendrick, *Molecular Physics*, 2005, **103**, 719–747.
- 37 S. Pronk, S. Páll, R. Schulz, P. Larsson, P. Bjelkmar, R. Apostolov, M. R. Shirts, J. C. Smith, P. M. Kasson, D. van der Spoel, B. Hess and E. Lindahl, *Bioinformatics*, 2013, **29**, 845–854.